

Time-domain-induced polarization: Full-decay forward modeling and 1D laterally constrained inversion of Cole-Cole parameters

Gianluca Fiandaca¹, Esben Auken², Anders Vest Christiansen³, and Aurélie Gazoty²

ABSTRACT

Time-domain-induced polarization has significantly broadened its field of reference during the last decade, from mineral exploration to environmental geophysics, e.g., for clay and peat identification and landfill characterization. Though, insufficient modeling tools have hitherto limited the use of time-domain-induced polarization for wider purposes. For these reasons, a new forward code and inversion algorithm have been developed using the full-time decay of the induced polarization response, together with an accurate description of the transmitter waveform and of the receiver transfer function, to reconstruct the distribution of the Cole-Cole parameters of the earth. The accurate modeling of the transmitter waveform had a strong influence on the forward response, and we showed that the difference between a solution using a step response and a solution using the accurate modeling often is above 100%. Furthermore, the presence of low-pass filters in time-domain-induced

polarization instruments affects the early times of the acquired decays (typically up to 100 ms) and has to be modeled in the forward response to avoid significant loss of resolution. The developed forward code has been implemented in a 1D laterally constrained inversion algorithm that extracts the spectral content of the induced polarization phenomenon in terms of the Cole-Cole parameters. Synthetic examples and field examples from Denmark showed a significant improvement in the resolution of the parameters that control the induced polarization response when compared to traditional integral chargeability inversion. The quality of the inversion results has been assessed by a complete uncertainty analysis of the model parameters; furthermore, borehole information confirm the outcomes of the field interpretations. With this new accurate code in situ time-domain-induced polarization measurements give access to new applications in environmental and hydrogeophysical investigations, e.g., accurate landfill delineation or on the relation between Cole-Cole and hydraulic parameters.

INTRODUCTION

During the last decade, the scope of time-domain-induced polarization (TDIP) has considerably broadened from mineral exploration to environmental geophysics, e.g., for clay and peat identification and lithological discrimination (Slater and Lesmes, 2002; Slater and Reeve, 2002; Kemna et al., 2004), landfill characterization (Weller et al., 1999; Dahlin et al., 2003) and detection of soil contamination (Vanhala, 1997; Kemna et al., 2004). Furthermore, modern instruments allow multichannel acquisition of induced polarization (IP) data with multicore cables and steel electrodes (Dahlin et al., 2002).

Although many developments have been seen in instrument design and acquisition techniques, the inversion schemes commonly

used still do not consider all the benefits of these improvements: TDIP data usually are inverted using the integral chargeability alone (Oldenburg and Li, 1994), without considering the actual transmitter waveform and the system transfer function of the receiver. However, the incomplete description of the transmitter waveform causes dramatic errors in the estimation of the magnitude and time characteristic of the IP phenomenon, as evident when studying the variability of the TDIP response to an infinite train of current pulses by changing the pulse duration (Tombs, 1981; Johnson, 1984).

In addition, the shape of the IP decay contains the spectral information of the IP phenomenon that may be extracted only by using

Manuscript received by the Editor 16 June 2011; revised manuscript received 5 January 2012; published online 23 April 2012.

¹University of Palermo, Department of Mathematics and Informatics, Italy. Visiting Researcher at the Hydrogeophysics Group, Aarhus University, Department of Geoscience, Denmark. E-mail: gianluca.fiandaca@unipa.it; gianluca.fiandaca@geo.au.dk.

²Aarhus University, Hydrogeophysics Group, Department of Geoscience, Denmark. E-mail: esben.auken@geo.au.dk; aurelie.legaz@geo.au.dk.

³Geological Survey of Denmark and Greenland, GEUS, Denmark. E-mail: anders.vest@geo.au.dk.

© 2012 Society of Exploration Geophysicists. All rights reserved.

the full decay in the inversion process. The rising importance of the IP spectral content in hydrogeophysics and hydrology is shown by several recent studies that correlate the time characteristics of the IP to the hydraulic conductivity of the soil in the laboratory (e.g., Bingley et al., 2005; Revil and Florsch, 2010; Titov et al., 2010). Some approaches have been presented that use the entire IP decay instead of the integral chargeability to resolve the Cole-Cole parameters (Cole and Cole, 1941; Pelton et al., 1978), by inverting the time gates independently with DC algorithms and interpreting the resulting time-dependent resistivity of each inversion cell as the response of a homogeneous space (Yuval and Oldenburg, 1997; Höning and Tezkan, 2007). Even if this approximation works well in a wide range of parameter contrasts (Hordt et al., 2006), the shape of the transmitter waveform and the receiver transfer function are not considered. Furthermore, the time-dependent resistivity series obtained in the first step of the inversion process do not necessarily obey the physics of the IP phenomenon because the different noise levels and resolution of the independent DC inversions may result in unrealistic decays.

Another procedure adopted to invert TDIP data uses the linearity of the IP phenomenon (Shuey and Johnson, 1973) and the resulting equivalence between the time domain and the frequency domain approaches. TDIP data are transformed in frequency domain through the Fourier transform and inverted by means of complex resistivity (CR) inversion algorithms (Weller et al., 1996; Kemna et al., 2000). Usually TDIP field data acquired with commercial instruments present a limited time range and a high noise content, making the Fourier transform unfeasible. Consequently, the usual transformation assumes a constant phase angle (CPA) model for the complex resistivity (Van Voorhis et al., 1973; Borner et al., 1996) that implies the proportionality between the frequency domain phase shift and the time domain integral chargeability.

For these reasons, a new forward code and an inversion algorithm have been developed using the full-time decay of the IP response, together with an accurate description of the transmitter waveform and of the receiver transfer function to reconstruct the distribution of the four Cole-Cole parameters of the earth. Synthetic examples and field examples from Denmark show a significant improvement in the resolution of the parameters that describe the IP response as compared to traditional integral chargeability inversion.

FORWARD RESPONSE

The main purpose of this study is to develop an inversion algorithm which can retrieve accurate values for the parameters describing the TDIP phenomenon. For this reason, it is critical to recognize the most significant aspects of the TDIP measurement procedure to be taken into account to compute an appropriate forward response. In the following, an accurate forward response is presented for layered media described by the Cole-Cole model, together with the main features of the measurement procedure to be modeled to refine the computations. In particular, in the section on transmitter waveform, the effects of the pulse duration and stacking procedure are presented. These effects have been treated in literature, e.g., in Tombs (1981) and Johnson (1984), but often are overlooked in the recent studies on IP inversion. Furthermore, in this study, the stacking procedure is treated with the focus on the small numbers of repetitions usually used with modern multichannel TDIP instruments. The enhanced speed of the modern acquisition systems is also the reason for which the quadrupole sequence effect becomes

significant and the standard deviation computed from the pulse stacking deviates from a real noise measurement, as shown in the following sections. To our knowledge, the latter effects, as well as the gate integration and receiver filter effects dealt with in this study, have not been treated in literature before.

1D step response for layered media described by the Cole-Cole model

The frequency variability of the complex resistivity adopted in this study follows the Cole-Cole model that often describes soil impedance exhaustively and that has been widely applied in the inversion of TDIP data (e.g., Yuval and Oldenburg, 1997; Höning and Tezkan, 2007) and spectral-induced polarization (SIP) data (e.g., Yoshioka and Zhdanov, 2005; Loke et al., 2006; Ghorbani et al., 2007; Chen et al., 2008).

The model space for the 1D forward response is defined as

$$\mathbf{m} = \{\rho_j, m_{0j}, \tau_j, c_j, thk_j\} j = 1, N_{Layers}, \quad (1)$$

where in the j th layer (of thickness thk_j), ρ_j represents the DC resistivity and m_{0j} , τ_j , and c_j are the Cole-Cole parameters needed to compute the electrical complex resistivity ζ_j of the layer as in Pelton et al. (1978):

$$\zeta_j(\omega) = \rho_j \left[1 - m_{0j} \left(1 - \frac{1}{1 + (i\omega\tau_j)^{c_j}} \right) \right]. \quad (2)$$

In equation 2, m_0 is the intrinsic chargeability as defined in Seigel (1959), τ is the relaxation time and c is the frequency exponent.

Once the complex resistivity of each layer is defined in terms of the Cole-Cole parameters, it is possible to compute the transfer function, $K(\omega, r, m)$, of the pole-pole forward response in the frequency domain by the well-known recurrence relations described in Koefoed (1979), as a function of pole-pole distance r , the frequency ω and the model vector \mathbf{m} . Note, in this work we have chosen to focus on the Cole-Cole model, but any kind of relation can be used in equation 2 to link polarization parameters and complex resistivity. For now, the Cole-Davidson model (Davidson and Cole, 1951) and the constant phase angle (CPA) model, as defined in Van Voorhis et al. (1973) have been implemented in our forward and inversion algorithms to supplement the Cole-Cole model.

Once the frequency domain transfer function $K(\omega, r, \mathbf{m})$ is computed, the time domain switch-off step response, V_{STEP} , is computed for an arbitrary quadrupole $ABMN$ on the surface by superposing the four poles responses obtained from the Fourier transform of the kernel $K(\omega, r, \mathbf{m})/i\omega$

$$V_{STEP}(t, ABMN, \mathbf{m}) = \begin{cases} \sum_{n=1}^4 (-1)^n K(\omega = 0, r_n, \mathbf{m}) & t \leq 0 \\ \sum_{n=1}^4 (-1)^n \left[K(\omega = 0, r_n, \mathbf{m}) - \int_0^\infty -\text{imag} \left(\frac{K(\omega, r_n, \mathbf{m})}{i\omega} \right) J_{1/2}(\omega t) d\omega \right] & t > 0 \end{cases} \quad (3)$$

where $\mathbf{r} = [AN, AM, BM, BN]$, i represents the imaginary unit and the Fourier transform is expressed with a Hankel transform of the imaginary part of the kernel in terms of $J_{1/2}$, i.e., the Bessel function of order 1/2.

In the algorithm for the forward response, the integrals contained in the frequency domain kernel and in equation 3 are computed by means of the fast Hankel transform presented by Johansen and

Sørensen (1979). To decrease the computation time, $K(\omega, r, \mathbf{m})$ and $V_{\text{STEP}}(t, \mathbf{ABMN}, \mathbf{m})$ are calculated for fixed (log-spaced) values of the variables r and t , respectively. In this way, the Hankel filter coefficients can be saved in tables and the number of Kernel computations is reduced, while the actual distances and times defining the quadrupoles and decays are computed by means of cubic splines.

The accuracy of this implementation of the step response for layered media has been tested by comparing it to the step response for the homogeneous half-space developed by Pelton et al. (1978). Figure 1 shows the comparison for an illustrative model ($m_0 = 100 \text{ mV/V}$, $\tau = 2 \text{ s}$, and $c = 0.5$). The IP decay is plotted following equation 4, to decouple the magnitude of the decay from the resistivity value:

$$M_{\text{STEP}}(t) = \frac{V_{\text{STEP}}(t)}{V_{\text{STEP}}(0)}. \quad (4)$$

The accuracy of our approach is controlled by the number of frequencies per decade used in the time-domain fast Hankel transform; with 10 points per decade, the relative error is below 10^{-3} , with 14 points per decade it is below 10^{-5} (Figure 1).

Gate integration

For conventional TDIP instruments, the voltage signal is averaged in time gates $[t_i, t_{i+1}]$ to reduce the noise content (Johnson, 1984). The recorded values M_i , are usually, like in equation 4, the ratio between the decay voltages and the DC voltage measured during the current on-time:

$$M_i = \frac{\int_{t_i}^{t_{i+1}} V(t') dt' / (t_{i+1} - t_i)}{\int_{t_s}^{t_e} V(t') dt' / (t_e - t_s)}. \quad (5)$$

Where t_s and t_e are the starting and ending time of the averaging interval in the on-time for the DC measurement.

Log-gating, which invokes logarithmically increasing window lengths with time, has been routinely used for electromagnetic (EM) time-domain induction methods to increase signal-to-noise ratios at late times. Log-gating is equally important in TDIP to decrease the noise level at later times by integrating the decreasing signal levels over increasing window lengths, but it is not yet a standard practice.

As long as the time gates are approximately log distributed and densely sampled (e.g., ten points per decade), it is a good approximation to skip the integration by computing the signal in the center of the gate (center calculated with the geometric mean), as shown also for EM methods in Becker and Cheng (1988) and Christiansen et al. (2011). In this case, the computation of equation 5 for the step response reduces to:

$$M_i \cong \frac{V_{\text{STEP}}(\sqrt{t_{i+1}t_i})}{V_{\text{STEP}}(0)}. \quad (6)$$

This approximation typically leads to relative errors in computations below 10^{-3} (e.g., for the model of Figure 1).

Transmitter waveform

In this study, “transmitter waveform” indicates the injected current waveform that energizes the subsurface. The transmitter

waveform differs from the ideal step current for two reasons: The switch-on (and switch-off) time of the current is not infinitesimal, and the full waveform is composed by a sequence of pulses of finite time length. The typical switching time of modern TDIP instruments is on the order of few tens of microseconds. For example, laboratory measured switch-on and switch-off times for the Syscal Pro equipment (Iris Instruments) are $55 \pm 5 \mu\text{s}$ in a current range between 10 and 300 mA. Considering that the minimum selectable time t_1 of the first time gate $[t_1 t_2]$ is typically a few milliseconds (e.g., 20 ms for the Syscal Pro equipment), the finite time length of switch-on (or switch-off) has a negligible influence on the voltage output and is not treated in details in the present study.

On the contrary, the finite duration of the current pulse and the stacking procedure have a dramatic effect on the forward response. Typically, IP signals need seconds, or tens of seconds, to completely decay, but in the field, the duration of the on-time current pulse T_{on} rarely exceeds the decay time.

The result of this is that the pulse response, obtained by superposing two time-shifted step responses of opposite sign, has a smaller amplitude and a faster decay compared to the step response. For instance, for the model used in Figure 1 with $T_{\text{on}} = 4 \text{ s}$, the initial amplitude of the pulse response is about 2/3 of the step response and the signal decays to 50% three times faster (Figure 2).

The typical way of measuring TDIP is to apply a sequence of alternating current pulses and to stack the signals (subtracting the signals with opposite sign to suppress self-potentials). In the stacking procedure, the j th voltage signal due to the stacked influence of j alternating current pulses can be expressed in terms of superposition of step responses (Figure 3a):

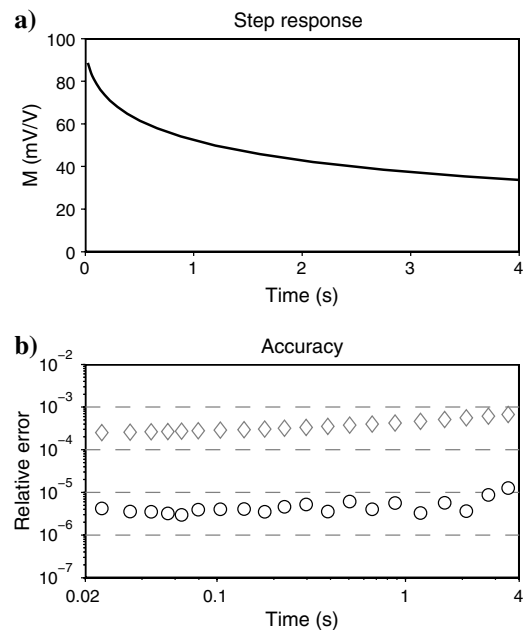


Figure 1. (a) Step response for a homogeneous half-space described by the set of Cole-Cole parameters ($m_0 = 100 \text{ mV/V}$, $\tau = 2 \text{ s}$, and $C = 0.5$). (b) Relative error of the forward response described in equation 3 in comparison with the homogeneous half-space implementation of Pelton et al. (1978); diamonds and circles represent the error obtained by using 10 and 14 points per decade in the fast Hankel time transform, respectively.

$$V_{STACK(j)}(t) = \sum_{m=1}^j \sum_{k=1}^2 (-1)^{m+k} V_{STEP}(t + (k-1)T_{ON} + (j-m)(T_{ON} + T_{OFF})), \quad (7)$$

where T_{on} represents the duration of the on-time current pulse and T_{off} is the time between consecutive pulses in which the IP measurements are carried out. The different stacks, arising from the superposition of different numbers of pulse responses, are different from each other, as shown in Figure 3b and 3c. Finally, equation 8 shows the formula for the averaged potential that can be substituted in equation 5 for the computation of the chargeability:

$$V_A(t) = \frac{1}{N_S} \sum_{j=1}^{N_S} (-1)^{j+1} V_{STACK(j)}(t), \quad (8)$$

where V_A is the averaged potential and N_S represents the number of stacks. The stacking procedure expressed in equation 8 not only decreases the noise content and suppresses self-potentials, but averages decays that are different. For this reason, the number of stacks affects the resulting signal and has to be properly modeled.

The formula for V_A holds for the off-time and on-time part of the signal and should be used to compute also the apparent resistivity ρ_a :

$$q_a = \frac{K_{ABMN}}{I} \frac{\int_{t_s}^{t_e} V(t') dt'}{(t_e - t_s)}, \quad (9)$$

where K_{ABMN} is the geometrical factor, I is the injected current, and t_s and t_e represent the range of integration for the DC measurement. The response dependency on the number of stacks is more pronounced for a small number of stacks when the stacks are more different from each other. Unfortunately, in 2D or 3D soundings for which thousands of quadrupole measurements are carried out, compromises are needed to maintain a reasonable acquisition time. In those cases, four or six stacks often represent the trade-off. For more repetitions, the infinite train assumption described by Tombs (1981) can be a good approximation of the real number of stacks, depending on the actual decay times and on the values of T_{on} and T_{off} .

Consider a measurement with six stacks on the homogeneous half-space described by the Cole-Cole parameters ($m_0 = 100 \text{ mV/V}$, $\tau = 2 \text{ s}$, and $C = 0.5$). Figure 4 shows the effect of

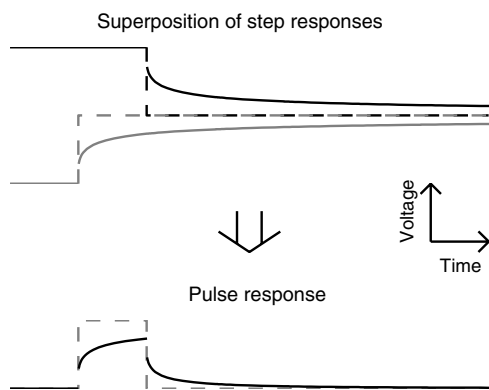


Figure 2. Construction of the pulse response by superimposing two-step responses.

underestimating the number of stacks in the computation of the forward response: At least four stacks are necessary to obtain accuracy below 1%. Figure 4 also shows the pure step response, which is between 60% and 400% different. This step response is what is used in conventional modeling of integral chargeability. The implementation of the actual waveform in the forward response also affects the DC resistivity value if the DC value is measured while the ground is not fully charged. Figure 5 displays the DC percentage difference versus the number of stacks for a homogeneous half-space described by ($\rho = 20 \text{ Ohm-m}$, $m_0 = 100 \text{ mV/V}$, $\tau = 2 \text{ s}$, and $C = 0.5$). The error on the DC value is, in this case, around 5% and it is driven by the m_0 parameter. With m_0 values well above 100 mV/V , which, for instance, is typical in landfills, the DC correction becomes severe.

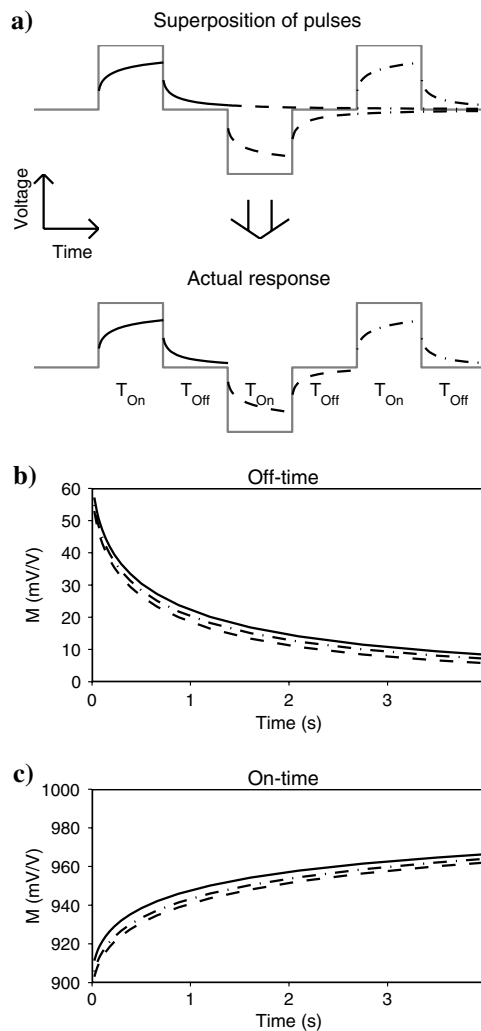


Figure 3. (a) Construction of the stacks by superposition of pulse responses. (b) Off-time decays for different stacks. (c) On-time charge up for different stacks. The IP signals are expressed in terms of equation 5 and refer to a homogeneous half-space described by the Cole-Cole parameters ($m_0 = 100 \text{ mV/V}$, $\tau = 2 \text{ s}$, and $C = 0.5$), as in Figure 1; the on- and off-times used for the waveform are: $T_{on} = T_{off} = 4 \text{ s}$. Solid lines, dashed lines and dotted-dashed lines correspond to the signal of the first, second and third current injection, respectively.

Quadrupole sequence and linear drift removal

The use of TDIP instruments that automatically switch between consecutive quadrupoles in the acquisition sequence significantly reduces the time between successive measurements. Consequently, the IP signal of each quadrupole in the sequence can be influenced by those arising from the former current injections, as stated in the following equation

$$V_{quad(n)}(t) = V_A^{AB(n)MN(n)}(t) + \frac{1}{N_S} \sum_{j=1}^{n-1} \sum_{k=1}^{N_S} (-1)^{k+1} V_{STACK(N_S)}^{AB(j)MN(n)}(t + T_{dly}), \quad (10)$$

where the (averaged) potential of the n th quadrupole measure $V_{quad(n)}$ is the sum of two terms: the potential originated by the n quadrupole itself, expressible by equation 8, and the potential arising from all the previous quadrupoles in the sequence, that depends also on the switching time between consecutive measurements T_{SWITCH} . In equation 10, $T_{dly} = (T_{SWITCH} + T_{OFF} + (k - 1)(T_{ON} + T_{OFF}) + (n - j - 1)(2T_{ON} + 2T_{OFF} + T_{SWITCH}))$.

When one of the electrodes of the injecting dipole $AB(j)$ of equation 10 coincides with one of the electrodes of the potential dipole $MN(n)$, the quadrupole sequence effect becomes dramatic and it takes several minutes after the current injection for the influence on the $AB(n)MN(n)$ quadrupolar measure becoming negligible. This special case of the quadrupole sequence effect is well-known in literature and it is usually named electrode polarization effect. It is common practice to design the TDIP acquisition sequence to maximize the time of reuse of an electrode for potential measurements after being used for current injection (Dahlin and Zhou, 2006). In the other cases, the effect of the quadrupole sequence is mainly due to the influence of the $n - 1$ th quadrupole measurement on the n th measurement, and its magnitude depends on the following factors:

- The effect decreases with increasing T_{SWITCH} , T_{ON} , T_{OFF} , and N_S (and then increasing the acquisition time of the survey).

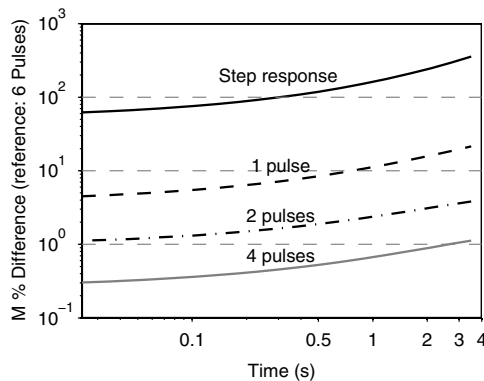


Figure 4. The IP percentage difference between decays with different number of stacks (the decay with six stacks being used as reference) for the homogeneous half-space described by the Cole-Cole parameters ($m_0 = 100$ mV/V, $\tau = 2$ s, and $C = 0.5$). Solid black line is step response. Dashed line is 1 pulse. Dotted-dashed line is two pulses. Gray solid line is four pulses. The on- and off-times used for the waveform are: $T_{on} = T_{off} = 4$ s. Note that the % axis is logarithmic.

- The effect increases when raising the ratio between $V_{STEP}^{AB(n-1)MN(n)}$ and $V_{STEP}^{AB(n)MN(n)}$, e.g., when the ratio between the quadrupole currents I_n/I_{n-1} decreases, or when $K^{AB(n)MN(n)}/K^{AB(n-1)MN(n)}$ increases (where K is the geometrical factor).

In the survey design, a compromise has to be established between the acquisition time and the magnitude of the effect of the quadrupole sequence; care can be used to build quadrupole sequences with decreasing geometrical factors. Typically, the effect of the quadrupole sequence on the TDIP forward response is only a few percent, but when the ratio between the currents I_{n-1} and I_n is significantly greater than one, the effect becomes severe. Figure 6 shows a typical example of quadrupole sequence effect, where the quadrupolar measurement ABMN is influenced by the signal A^*B^*MN arising from the previous measurement in the quadrupole sequence. Figure 6a shows a sketch of the transmitter waveforms of the quadrupoles, with four pulses, $T_{on} = T_{off} = 4$ s and $T_{SWITCH} = 1$ s (1 s for switching the quadrupole sequence is a typical value, for instance, for the Syscal Pro equipment). Figure 6b shows a quantitative plot of the four stacks of the IP decays for the ABMN quadrupole (solid gray lines) and the signals A^*B^*MN (dashed gray lines) for the model and the quadrupoles described in Figure 6c. The signals represented by the solid and dashed gray lines in Figure 6b are all normalized by the DC value of the ABMN quadrupole and expressed in mV/V, instead of in volt (without normalization) to simplify the understanding of the y-axis scale. In Figure 6b, the dashed black line represents the cumulative effect of the four A^*B^*MN signals, whereas the dotted-dashed black line represents the same effect when the current $I_{A^*B^*}$ of the former quadrupole is ten times the current I_{AB} of the subsequent quadrupole. Finally, Figure 6d shows the ABMN decay not affected by the previous quadrupole (solid gray line), affected by the previous quadrupole with $I_{A^*B^*}/I_{AB} = 1$ (dashed black line) and affected by the previous quadrupole with $I_{A^*B^*}/I_{AB} = 10$ (dotted-dashed black line). On average, on the entire decay, the quadrupole sequence effect causes a 3% modification with $I_{A^*B^*}/I_{AB} = 1$ and a 33% modification with $I_{A^*B^*}/I_{AB} = 10$ for the ABMN forward response of Figure 6c.

The effect of the quadrupole sequence can be reduced not only by increasing the acquisition time but also by changing the pulse

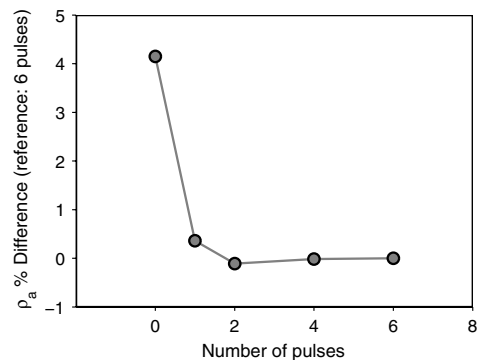


Figure 5. The DC percentage difference between measures with different number of stacks (the measure with six stacks being used as reference) for the homogeneous half-space described by the Cole-Cole parameters ($m_0 = 100$ mV/V, $\tau = 2$ s, and $C = 0.5$). The on- and off-times used for the waveform are: $T_{on} = T_{off} = 4$ s.

sequence. While the alternating sequence of current pulses automatically removes only constant potentials present between the electrodes, the sequence obtained repeating one positive, two negative, and one positive pulses (+ - -+) performs the linear drift removal. The pulse sequence also affects the forward response without considering the effect of the quadrupole sequence. Consequently, the correct pulse sequence, or other algorithms for linear drift removal usually adopted in the resistivity-meters, have to be modeled in the forward response.

Low-pass filters in the receiver

Yet another significant aspect to be taken into account to perform an accurate computation of the TDIP forward response is the presence of low-pass filters in TDIP instruments. For example, in the widely used Syscal Pro receiver (Iris Instruments), a nominal 10 Hz low-pass digital Gaussian filter is present to reduce the 50 Hz interferences on the IP signal and to reduce noise. This filter disturbs the early times with up to several hundreds percent and it must be added in equation 3 (Effersø et al., 1999).

Figure 7 shows the effect of the Syscal Pro filter in the time domain and its modeling in the forward response for an illustrative

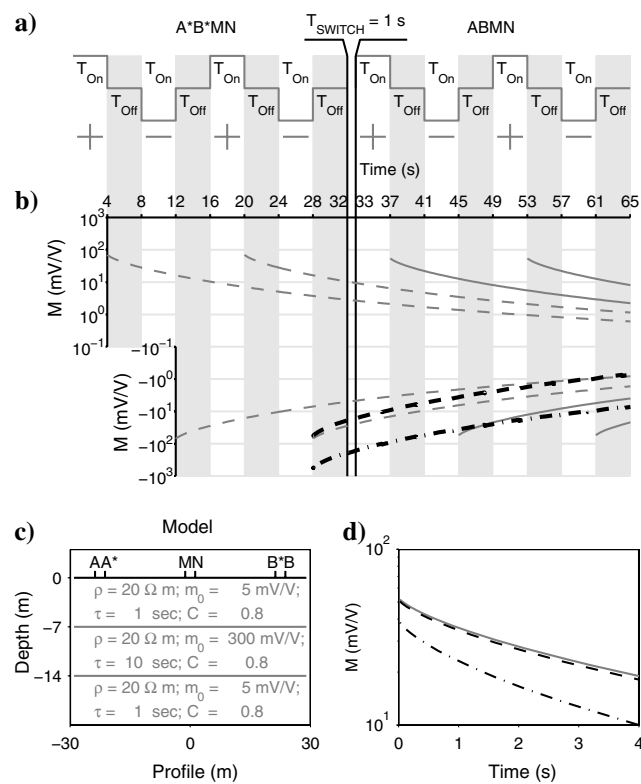


Figure 6. (a) Sketch of the transmitter waveforms of two consecutive quadrupolar measurements. (b) Dashed gray lines are potential signals originated by the A*B*B* current pulses. Dashed black line is overall A*B*B* effect by superposition of the dashed gray lines. Dotted-dashed black line is overall A*B*B* effect with a ratio between the A*B*B* and AB currents $I_{A*B*}/I_{AB} = 1$. Solid gray lines are potential signals originated by the AB current pulses. Note that the y axis is logarithmic. (c) Model and quadrupoles description. (d) Continuous gray line is ABMN decay with $I_{A*B*}/I_{AB} = 0$; Dashed black line is ABMN decay with $I_{A*B*}/I_{AB} = 1$. Dotted-dashed black line is ABMN decay with $I_{A*B*}/I_{AB} = 10$.

model (homogeneous half-space with $m_0 = 100 \text{ mV/V}$, $\tau = 2 \text{ s}$, and $C = 0.5$). The filter modeling necessitated the superposition of five Gaussian filters (i.e., filters described by a characteristic expressed in terms of a real Gaussian function) with central frequencies between 4 and 10 Hz, instead of the single 10 Hz nominal one. Without the filter modeling all the measures before, 80–100 ms should be rejected in the inversion process with a significant loss of information in the early times corresponding to high frequencies.

Standard deviation and noise content

The last feature of the TDIP forward response discussed in this study regards the standard deviation of IP signals. Consider the simple three-layer model shown in Figure 8a (the same as Figure 6c). Four different IP measurements have been simulated on it (always with four stacks and $T_{\text{ON}} = T_{\text{OFF}} = 4 \text{ s}$):

- 1) the quadrupolar measurement ABMN, obtained by stacking four alternating current pulses + - -+ (Figure 8b, continuous gray line);
- 2) the quadrupolar measurement ABMN affected by a previous current injection between the electrodes A*B*B* (computed with $T_{\text{SWITCH}} = 1 \text{ s}$ and $I_{n-1} = I_n$), obtained by stacking four alternating current pulses + - -+ (Figure 8b, dashed gray line);

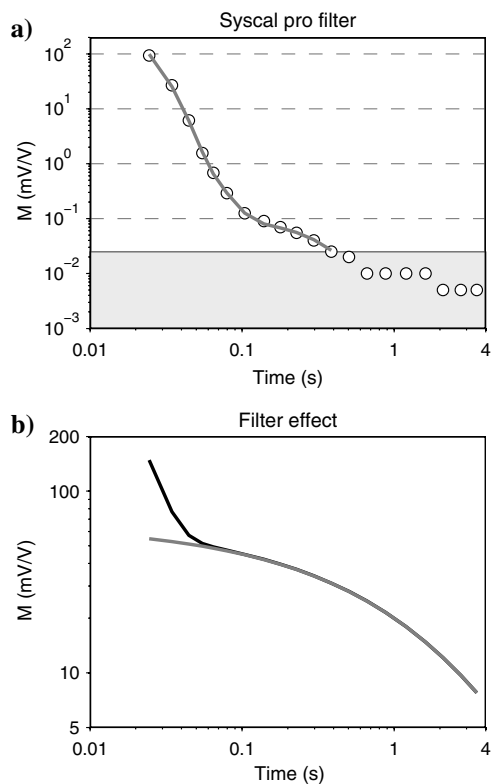


Figure 7. (a) Syscal Pro filter effect (circles) measured in time domain on a nonchargeable resistor. The gray line represents the modeling of the filter, for which the measures in the gray rectangle are not been taken into account (because the limit of the digitalization of the data has been reached). (b) Black line is the forward response with the filter implementation; gray line is the forward response without the filter implementation. The decays have been computed for the homogeneous half-space described by the Cole-Cole parameters ($m_0 = 100 \text{ mV/V}$, $\tau = 2 \text{ s}$, and $C = 0.5$). The on- and off-times used for the waveform are: $T_{\text{on}} = T_{\text{off}} = 4 \text{ s}$, six stacks.

- 3) the quadrupolar measurement ABMN, obtained by stacking four current pulses for the linear drift removal + - - + (Figure 8b, continuous black line);
- 4) the quadrupolar measurement ABMN affected by a previous current injection between the electrodes A*B* (computed with $T_{\text{SWITCH}} = 1$ s and $I_{n-1} = I_n$), obtained by stacking four current pulses for the linear drift removal + - - + (Figure 8b, dashed black line);

The standard deviation computed on different stacks for noise-free data easily reaches and exceeds the value of 10%, and the effect of the quadrupole sequence strongly influences the results. For the alternating pulse sequence example, the signal coming from the former current injection completely compensates the stacks variability, with a standard deviation averaged on the entire decay that goes from 12% (without taking into account the previous injection, Figure 8c) to 0.3% (Figure 8d). On the contrary, for the pulse sequence that performs the linear drift removal, the standard deviation increases considering the quadrupole sequence, going from 22% (Figure 8e) to 26% (Figure 8f).

These simple examples show clearly that the standard deviation computed from the stacking procedure is not a good measure of the noise content of the data, reaching high levels also for noise-free decays. This effect can be less pronounced for the alternating pulse sequence when the compensation due to the quadrupole sequence plays a role. But, again, the compensation depends on unknown or unpredictable parameters, like the distribution of the Cole-Cole parameters and the values of the injected current for different quadrupoles.

INVERSION

The aim of the inversion scheme presented in this study is to extract the spectral content of the IP phenomenon from time domain measurements. The spectral information is contained in the time decays. Therefore, all decay samples at the different time gates have to be included in the data space. In the model space, the description of the spectral information is obtained using the Cole-Cole model (Pelton et al., 1978), i.e., including the resistivity and the parameters describing the frequency dependency. Other approaches for 1D/2D inversion use the same data and model spaces, but compute the forward response in a two-step process (Yuval and Oldenburg, 1997; Höning and Tezkan, 2007): first, the apparent chargeability values are inverted for each time gate independently by means of a 1D or 2D DC algorithm, and then, for each layer/cell of the 1D/2D models, the resulting decays are inverted with the TD Cole-Cole formula for a homogeneous half-space (the values of the decays for different time gates being obtained from the independent DC inversions). On the contrary, in this study, the 1D forward response described in the previous section is directly used in the inversion and, consequently, the model parameters are simultaneously obtained in a unique inversion process where the relationship between parameters is maintained at all times.

The inversion in this paper has been implemented in the 1D laterally constrained inversion (LCI) scheme (Auken et al., 2005), retrieving 2D sections in quasi-layered environments.

1D-LCI implementation

In the 1D-LCI inversion algorithm, the model is composed of a set of laterally constrained 1D models aligned along a profile

(Auken et al., 2005), as sketched in Figure 9. In the TDIP implementation, the model space is set up with the logarithms of the Cole-Cole parameters and with the logarithms of the thicknesses for all the layers of each model:

$$m = (\{\log(\rho_{i,j}), \log(m_{0,i,j}), \log(\tau_{i,j}), \log(c_{i,j}), \log(thk_{i,k})\},$$

$$i = 1, N_{\text{models}}; j = 1, N_{\text{layers}}; k = 1, N_{\text{layers}} - 1). \quad (11)$$

The use of the logarithm of all the parameters in the inversion algorithm has not been guided by physical considerations, but is a pragmatic solution because our code allows the log transformation on all the parameters or none. The data set of quadrupole measurements can be both a collection of 1D soundings and a set of quadrupoles generated with arrays suited for 2D surveys. In the former case, one 1D model is built for each sounding; in the latter case, the

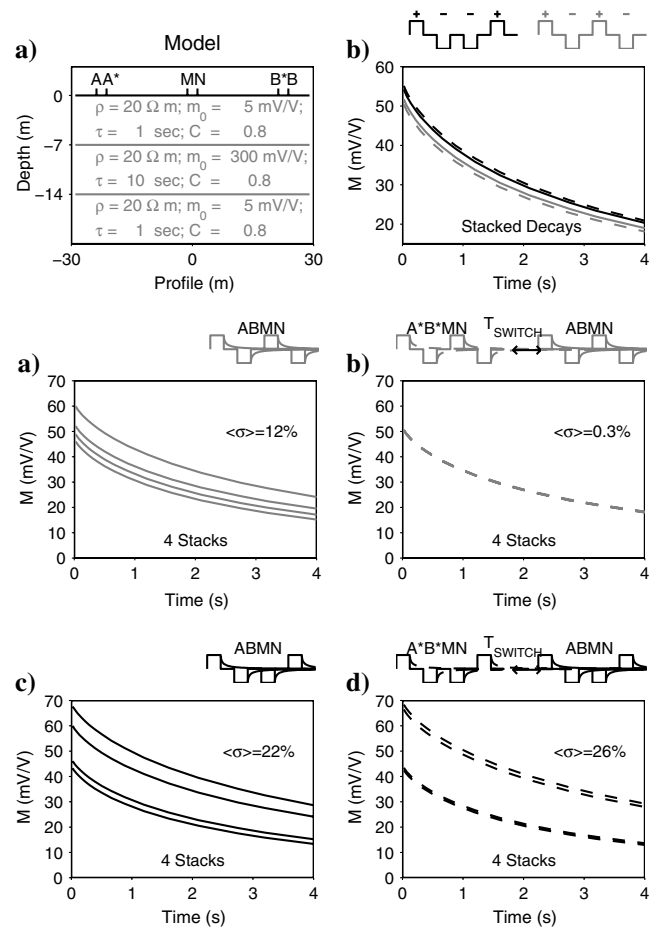


Figure 8. (a) Three-layer model of the earth. (b) Stacked signals for different pulse sequences ($T_{\text{on}} = T_{\text{off}} = 4$ s): Black lines are the linear drift removal sequences; gray lines are the alternating pulse sequences; dashed lines are the effect of the previous current injection A*B* taken into account ($T_{\text{SWITCH}} = 1$ s); continuous lines mean no previous current injection. (c) The four stacks for the alternating pulse sequence without previous current injection. (d) The four stacks for the alternating pulse sequence with previous current injection. (e) The four stacks for the linear drift removal sequence without previous current injection. (f) The four stacks for the linear drift removal sequence with previous current injection.

data set is split into several 1D soundings by using the distribution of the 2D sensitivity function (of resistivity) to compute the lateral focus point (LFP) of the quadrupoles (Møller et al., 1998; Auken et al., 2005).

With 2D data sets acquired by multichannel resistivity-meters, each 1D sounding typically contains all the measures with LFP located within one electrode spacing around the position of the corresponding 1D model.

The data space for the inversion is the logarithm of the apparent resistivity and the chargeability values (for all time gates) for every quadrupole (expressed in terms of equations 5 and 9):

$$d = (\{\log(\rho_{i,j}^a); \log(M_{i,j,k})\}, i = 1, N_{\text{models}}; j = 1, N_{\text{quads}(i)}; k = 1, N_{\text{gates}(i,j)}). \tag{12}$$

The 1D-LCI approach simultaneously inverts all data sets and constraints, minimizing a common objective function, but computing the forward responses (and the corresponding derivatives for the Jacobian) by means of the 1D solution. The lateral constraints set up between adjacent models assure the lateral migration of information among the models (Figure 9). Furthermore, constraints to the initial values (a priori information) of model parameters and vertical constraints are implemented in the inversion scheme, as well as constraints to the depths of layers (and not only to the thicknesses, e.g., to integrate borehole information).

The 1D-LCI approach works well in quasilayered environments, like in sedimentary areas, where it is rare that the 1D assumption is strongly violated in the sensitivity volume of the electrode configurations. In these cases, all the benefits of the inversion scheme presented in this study can be achieved in terms of the following:

- 1) Accuracy of the forward response, implemented with all the features described in the previous sections. The only approximations used in the inversion process are the center gate approximation described in equation 6 and the computation of the quadrupole sequence effect limited to the quadrupole $n - 1$ of equation 10.
- 2) complete usage of the acquired data, with all the time gates included in the data space, without any reduction of the spectral information content (that is lost using the approach of Oldenburg and Li [1994])
- 3) simultaneous inversion of resistivity and chargeability parameters, without any two-step approach (Oldenburg and Li, 1994) or independent inversion for different time gates (Hönig and Tezkan, 2007)

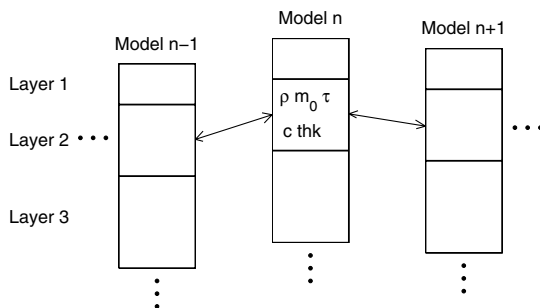


Figure 9. LCI model setup. The arrows represent the lateral constraints.

- 4) expansion of the model space including all the Cole-Cole parameters, to extract the spectral information contained in the time-domain decays
- 5) straightforward incorporation of a priori information, e.g., from boreholes
- 6) possibility of inverting for both layered models, with electrical parameters and thicknesses free to change during the inversion process, and smooth models, increasing the number of layers and adding vertical smoothness constraints between layers with a set of fixed thicknesses
- 7) computation of the uncertainty analysis of the inverted model parameters

A detailed description of the inversion algorithm and the practical implementation of the constraints is given by Auken and Christiansen (2004). The inversion is performed iteratively, by following the established practice of linearized approximation of the nonlinear forward mapping of the model to the data space, by the first term of the Taylor expansion. The objective function minimized in the inversion process is expressed by

$$Q = \left[\frac{[\delta d]^T C^{-1} \delta d}{N_d + N_m + N_R} \right]^{\frac{1}{2}}, \tag{13}$$

where C' is the covariance matrix of the inversion and $\delta d'$ is the data vector update. In equation 13, N_d , N_m , and N_R represent the number of data points, the number of model parameters, and the number of constraints. The output models are then balanced between the data (through the forward response, i.e., the physics), the a priori constraints, and the roughness constraints.

As suggested in Tarantola and Valette (1982b), the error in the theoretical description of the forward response can be introduced in the inverse problem formulation through the data covariance matrix. Therefore, in the 1D-LCI inversion scheme, a minimum value for the diagonal elements of the data covariance matrix is stated independently from the measured standard deviation to account for the model dimensionality approximation. Experimental tests on field data suggest a minimum threshold for the standard deviation of 5% on the resistivity values and 15% on the chargeability ones, more affected by the noise due to the smaller values of the measured potentials.

The inversion algorithm presented in this paper has been implemented in the em1dinv code (Christiansen and Auken, 2008), that handles several electrical and electromagnetical methods in the same framework and is free for the scientific community.

One-dimensional synthetic example

A Schlumberger sounding was simulated on the three-layer model described in Table 1. The sounding is composed of 20 quadrupoles, with approximately log-spaced AB/2 ranging from 3.75 m to 248.75 m; MN/2 ranges from 1.25 m to 33.75 m, to limit the geometrical factor to 3000 m. Four stacks were considered for each quadrupole, with $T_{on} = T_{off} = 4$ s. Twenty time gates, with width approximately log-distributed between 10 and 800 ms, were generated (the first center gate time being 24.5 ms). The filter effect was simulated, considering the filter characteristic of the Syscal Pro equipment discussed in Figure 7.

Gaussian noise with standard deviation equal to 10% and 3% of data values was added to the chargeability and resistivity values, respectively. The noise level was chosen to be so high to give

meaning to the uncertainty analysis even without a detailed modeling of the noise on the data, and it is comparable with the noise level in the field (Gazoty et al., 2011).

No a priori or vertical constraints were used for the inversion, carried out with three layers and three different forward modeling approaches:

- inversion without the implementation of the transmitter waveform (only step response) and without the filter effect in the forward modeling, hereafter STEP inversion
- inversion with the implementation of the transmitter waveform but without the filter effect in the forward modeling, hereafter W inversion
- inversion with the implementation of the transmitter waveform and with the filter effect in the forward modeling, hereafter WF inversion

In the inversions without the filter modeling, the first six gates of the IP decays were removed to avoid bias in the results. In all the inversions, a homogeneous starting model ($\rho = 10 \Omega\text{m}$, $m_0 = 10 \text{ mV/V}$, $\tau = 1 \text{ s}$, $c = 1$, $thh_1 = 1 \text{ m}$, and $thh_2 = 20 \text{ m}$) was used, and the stopping criterion for the inversion was a relative change in the objective function below 1%. On all the inversion results, the uncertainty analysis on the parameters was computed through the covariance of the estimator error for linear mapping C_{est} described by Tarantola and Valette (1982a). Because the model parameters are represented as logarithms, the analysis gives a standard deviation factor (STDF) for the i th parameter m_i defined by

$$\text{STDF}(m_i) = \exp\left(\sqrt{C_{est(i,i)}}\right). \quad (14)$$

Hence, under lognormal assumption, it is 68% likely that the i th model parameter m_i falls in the interval

$$\frac{m_i}{\text{STDF}(m_i)} < m_i < m_i \cdot \text{STDF}(m_i). \quad (15)$$

The inversion results are presented in Table 1. For all three inversions with different forward modeling approaches, the data misfit expressed via equation 13 is 1.1. Despite the good data fit, the STEP inversion strongly underestimates the m_0 and τ values of the second layer (the true values being more than twice the inversion ones), and the true values of the parameters are well outside the confidence interval obtained by the uncertainty analysis. On the contrary, the W inversion retrieves correctly, in terms of predicted values and confidence intervals, all the parameters of the synthetic models, even if the uncertainty is large (mean STDF = 1.8, averaged over all layers and parameters), especially in the first layer, where the τ value of true model is below the first center gate time (80 and 104 ms, respectively). Finally, the WF inversion, when compared to the W inversion, shows a large reduction of the uncertainty of all the inversion parameters (mean STDF = 1.3), and particularly in the first layer. The significant improvement in the first layer (with $\tau = 80 \text{ ms}$) shows that the implementation of the filter characteristics in forward response enhances the retrieval of spectral information even in the frequency range strongly affected by the filter.

The inversion shown is just an example; a complete study on the resolution of the Cole-Cole parameters is beyond the scope of this paper. However, the example illustrates realistic contrasts of parameters, such as those found in buried landfills (e.g., Auken et al., 2011). Furthermore, it does not take into account resistivity contrasts, to show the ability of the inversion to retrieve the right

Table 1. Description of a three-layer model and corresponding inversion results varying the forward modeling. Min and Max column headers stay for minimum and maximum values of the 68% confidence interval obtained by the uncertainty analysis of equation 13.

	True model	STEP inversion			W inversion			WF inversion		
	Value	Value	Min	Max	Value	Min	Max	Value	Min	Max
$\rho_1(\Omega\text{m})$	20	20.1	19.8	20.5	20.1	19.8	20.5	20.2	19.8	20.6
$\rho_2(\Omega\text{m})$	20	15.7	15.1	16.4	22.2	19.7	25.1	20.4	19.2	21.7
$\rho_3(\Omega\text{m})$	20	20.0	19.8	20.3	20.0	19.8	20.3	20.1	19.8	20.3
$m_0 \ 1(\text{mV/V})$	5	2.8	1.5	5.1	3.8	1.1	13.2	5.7	3.0	10.9
$m_0 \ 2(\text{mV/V})$	300	142	130	155	372	303	458	312	273	356
$m_0 \ 3(\text{mV/V})$	5	3.6	3.2	4.0	3.9	3.3	4.6	4.2	3.7	4.8
$\tau_1 \ (\text{s})$	0.08	0.15	0.07	0.35	0.10	0.01	0.73	0.06	0.02	0.16
$\tau_2 \ (\text{s})$	8	3.2	2.9	3.4	17.1	9.0	32.5	10.7	7.7	14.8
$\tau_3 \ (\text{s})$	1	0.9	0.8	1.2	1.0	0.9	1.2	0.9	0.8	1.1
$c_1 \ (\text{dimless})$	0.8	0.84	0.74	0.97	0.74	0.57	0.96	0.77	0.66	0.89
$c_2 \ (\text{dimless})$	0.8	0.72	0.68	0.76	0.69	0.63	0.75	0.75	0.71	0.79
$c_3 \ (\text{dimless})$	0.8	0.95	0.89	1.02	0.91	0.81	1.02	0.87	0.78	0.96
Thick1 (m)	7	7.0	6.7	7.2	6.9	6.7	7.1	6.8	6.6	7.0
Thick2 (m)	7	7.6	6.8	8.4	7.8	7.0	8.6	7.9	7.2	8.6
Depth1 (m)	7	7.0	6.7	7.2	6.9	6.7	7.1	6.8	6.6	7.0
Depth2 (m)	14	14.5	14.0	15.1	14.7	14.1	15.3	14.7	14.2	15.2

layer thicknesses from only the variation of the Cole-Cole parameters.

Ghorbani et al. (2007), using the Bayesian method, conclude that the resolution of TDIP for Cole-Cole parameters in a homogeneous half-space is really poor and that the linearized approach fails in retrieving reasonable error estimates because of the high nonlinearity of the forward mapping. Two differences between the approach followed in this study and the Ghorbani et al. (2007) approach can explain the different results:

- The correction due to the waveform implementation for the apparent resistivity values (using equation 8 in equation 9) has not been implemented in Ghorbani et al. (2007), whereas the waveform implementation has been used to compute the IP response. For this reason, models with different DC values have been considered equivalent in their approach.
- In Ghorbani et al. (2007), several illustrative models present the Cole-Cole time constant τ one order of magnitude smaller than the first time gate considered in the decay measurement. In these cases, the resolution of the TDIP method cannot be good.

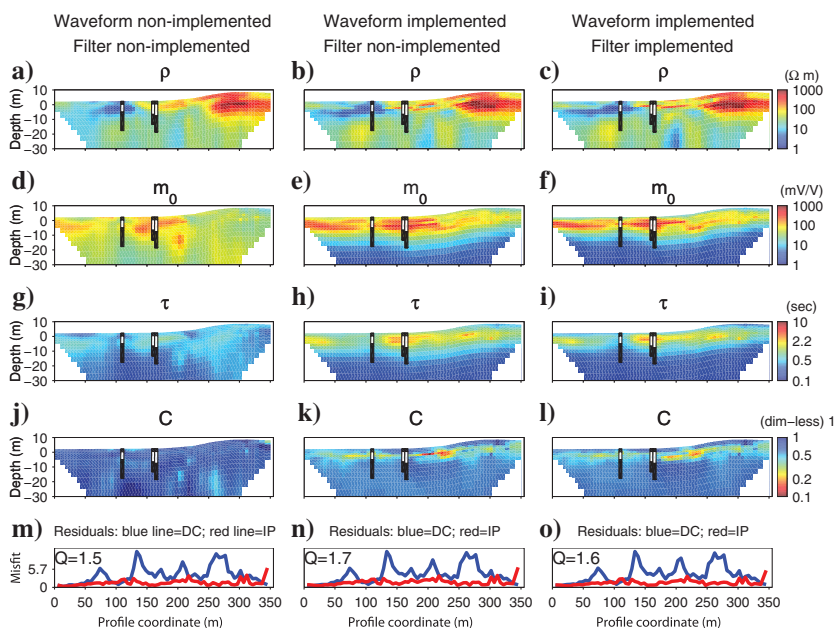
Field example

To evaluate the inversion scheme on a field example, a test site with borehole information was chosen. This is the Eskelund landfill site, in the vicinity of Aarhus, Denmark. The DC-IP sections shown in this paper correspond to one of the 13 profiles performed to delineate the landfill boundaries in the framework of the Cliwat project (an Interreg IVB North Sea Region Program). The survey was carried out with the Syscal Pro 72 equipment (Iris Instruments), with 72 electrodes and 5 m takeouts. The multiple gradient array (Dahlin and Zhou, 2006) was chosen to generate the quadrupole sequence. A total number of 1410 quadrupoles were used to perform the TDIP measurements: For each quadrupole, 20 TDIP time gates were acquired, approximately log-sampled between 10 and 800 ms. Four or six stacks were used for each measurement, depending on the noise content, with alternating current pulses ($T_{\text{on}} = T_{\text{off}} = 4$ s). After the re-

jection of outliers in the IP decays, 19,388 data points were used for the inversion, performed with 70 smooth 1D models with 19 layers, for a total number of inversion parameters equal to 5320. As in the synthetic example, the STEP, W, and WS inversions were carried out on the same data set. For all the parameters, the vertical constraints between adjacent layers were set up equal to 0.5 and the lateral constraints between adjacent models equal to 0.2, roughly allowing 50% vertical variation and 20% lateral variations between the constrained parameters. In fact, in the 1D-LCI implementation, the lateral and vertical constraints represent the relative variation of the parameters that weights the roughness misfit in the objective function Q through the covariance matrix C' of equation 13. No a priori constraints were imposed and a homogeneous starting model was used ($\rho = 20 \Omega\text{m}$, $m_0 = 1 \text{ mV/V}$, $\tau = 0.1 \text{ s}$, and $c = 1$). The stopping criterion used for the inversion is a relative change in the objective function below 1%. About fifteen minutes were necessary to perform the entire inversion (20 iterations), plus the uncertainty analysis on a 12-core machine (Intel Xeon E5520 CPU, 2.27 GHz), with the code being optimized for parallel computation using the open multi-processing (OpenMP) application programming interface (API).

Figure 10 shows the inversion results, with one section for each parameter. Three boreholes are superposed on the sections represented in grayscale. The white color corresponds to the waste body. The STEP inversion differs significantly from the W and WF inversions: the range of the inverted Cole-Cole parameters is considerably smaller, confirming the results of the synthetic example. Furthermore, the pattern of the chargeable anomaly is different in the m_0 sections, and the resistivity sections show discrepancies, mainly in the top 10 m between 150 m and 250 m along the profile. The differences between the W and the WF inversions are less pronounced, but there is a sharper vertical contrast in the m_0 section of the WF inversion. A clear correlation between the highly chargeable anomaly and the landfill is visible in the m_0 sections of the W and WF inversions, the match with the top and bottom vertical boundaries of the landfill being very good, whereas the match is poorer with the STEP approach. On the contrary, in all the resistivity sections, it is not possible to recognize the waste body, the landfill

Figure 10. Sections of the Cole-Cole parameters retrieved by the inversion of the DC-IP profile acquired at the Eskelund landfill. Three boreholes are shown in grayscale, the white color corresponding to the waste body.



extending in the resistive and in the conductive part of the profile. The τ and c sections present lateral variations of the parameters in the waste body, suggesting the existence of compositional heterogeneity. Like in the synthetic example, the total misfit, as defined in equation 13, is similar for all the inversions. The resistivity data misfit is quite pronounced at the boundaries of the resistive anomalies in the top sections of Figure 10, as clearly shown by the DC residuals plotted in the 10m:10o (blue lines).

Figure 11 shows the uncertainty analysis of the WF inversion of Figure 10, presented again with one section for each parameter. The dark blue areas of the sections correspond to an uncertainty equal or above the lateral constraint value of the inversion, indicating where the parameter retrieval is constraints (and not data) driven. It is then clear from Figure 11 that the depth of investigation for m_0 , τ , and c

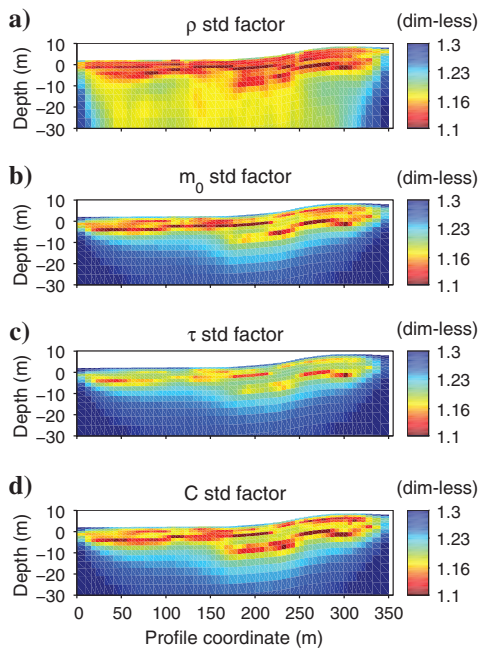


Figure 11. Uncertainty analysis (as defined in equation 14) for the Cole-Cole parameters obtained in the inversion of Figure 10c, 10f, 10i, and 10l.

is lower than the resistivity one, due to the higher noise content of the data.

Finally, a comparison between the WF and STEP inversion algorithms presented in this study and the RES2DINV code by Geotomo software (Loke and Barker, 1996) is presented in Figure 12. In RES2DINV, the chargeability is computed in a two-step algorithm by carrying out two DC resistivity forward mapping for the DC value and for the late time resistivity as described by Oldenburg and Li (1994). The parameters retrieved in the RES2DINV inversion are the resistivity and the integral chargeability, integrated over the entire range of acquisition of the IP signal. This approach does not take into account the actual waveform used to inject the current (like T_{on} , T_{off} , or the number of stacks), nor the filter characteristics of the Syscal instrument. Hence, RES2DINV inversions give different values for the chargeability just by changing the acquisition settings in the field. The RES2DINV inversion was carried out with robust data and model constraints and with the vertical to horizontal flatness filter ratio of 0.4, to help the recognition of horizontal structures. The stopping criterion for the inversion was a difference in the data misfit below 1% between consecutive iterations and the final RMS misfit was 1.8% for resistivity and 1.2% for integral chargeability.

To facilitate the comparison of the two approaches, the integral chargeability was computed also for our inversion scheme, by using the Cole-Cole parameters to calculate the decays. Consequently, the chargeability sections of Figure 12 are plotted in the same unit, with the same color scale. The STEP and the RES2DINV inversions are quite similar in terms of anomaly patterns and parameter values, in the resistivity sections (Figure 12a and 12b) and in the integral chargeability ones (Figure 12d and 12e), even if the RES2DINV inversion shows a patchier appearance in the chargeability section. The similarity between the STEP and RES2DINV inversions indicates that the 1D-LCI formulation does not prevent the retrieval of 2D structures, at least in quasi-layered environments. When comparing Figure 12d and Figure 12e, it is clear how the transmitter waveform implementation considerably changes the inversion results in terms of parameter values and anomaly patterns. Finally, the comparison between Figure 10 and Figure 12 shows the increased information content of the Cole-Cole inversion compared to the integral chargeability inversion. In fact, through the m_0 , τ , and c sections, it is possible to discriminate the factors that determinate the magnitude of the integral chargeability.

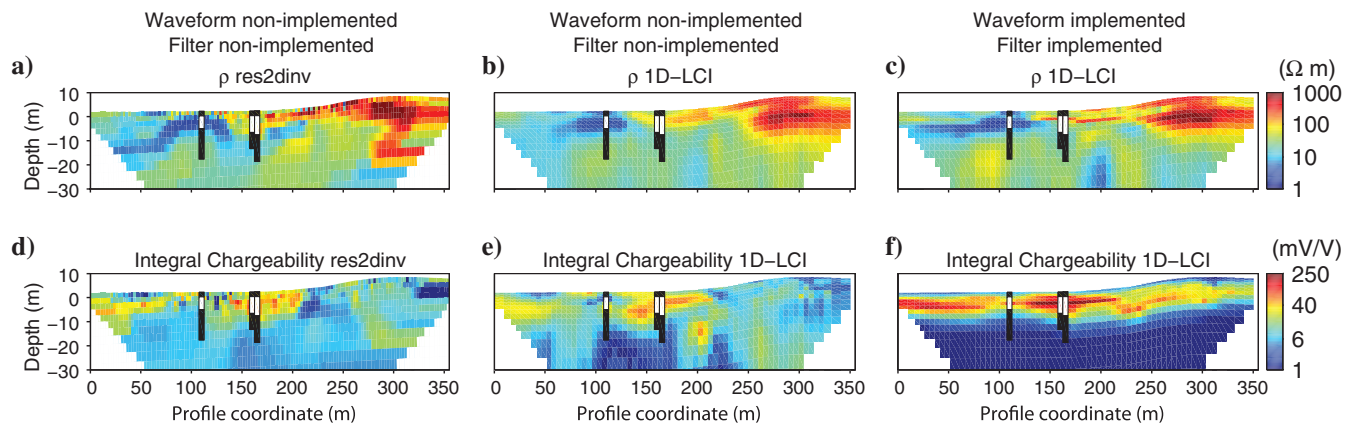


Figure 12. Comparison of RES2DINV and 1D-LCI inversions.

CONCLUSIONS

A new forward code and inversion algorithm have been developed using the full-time decay of the IP response, together with an accurate description of the transmitter waveform and of the receiver transfer function, to reconstruct the distribution of the four Cole-Cole parameters of the earth.

The implementation of an accurate forward modeling for TDIP that considers the detailed description of the sequence of current pulses applied to the ground, together with an appropriate modeling of the receiver transfer function, avoids significant bias in the retrieval of the model parameters. On the contrary, inaccurate descriptions of the acquisition system and settings introduce severe errors in the inverted values, usually with a strong underestimation of chargeability parameters describing the magnitude and the time scale of the IP phenomenon.

When the system description is adequate, the inversion scheme proposed in this study allows the Cole-Cole parameters of the subsurface to be retrieved and the uncertainty analysis suggests that time-domain decays contain enough information to resolve all the Cole-Cole parameters. Furthermore, the comparison between the RES2DINV and the 1D-LCI inversion results show that the 1D-LCI approach does not prevent the retrieval of 2D structures, at least in quasylayered environments. The RES2DINV approach does not allow the implementation of the transmitter waveform and receiver transfer function and gives significant bias in the parameter retrieval in terms of parameter ranges and anomaly patterns.

Although the presented work focuses solely on the Cole-Cole parameterization of the IP phenomenon, different a priori spectral models have been implemented in the forward modeling and inversion scheme by changing the formula that links the model parameters to the complex resistivity of the soil. Regardless of the chosen modeling for the complex resistivity, when considering the extraction of the spectral information of the polarization phenomenon from in field time domain data, it has to be remembered that with currently available TDIP resistivity meters, only two orders of magnitude in time are usually measured. On the contrary, in laboratory frequency domain studies, several orders of magnitude are explored: In these cases, models more complex than the Cole-Cole one are usually necessary to explain the data, also for homogeneous samples. Nevertheless, extracting the time characteristics of the polarization from in situ time-domain measurements gives access to new applications of TDIP in environmental and hydrogeophysical investigations, e.g., on the relation between IP parameters and hydraulic parameters. Considering that the transmitter waveform and the receiver transfer function have a large impact on the inverted spectral parameters, we believe that the improved modeling of TDIP data will allow for improving the link between field and laboratory studies, as well as the link between the time-domain and frequency-domain IP approaches.

ACKNOWLEDGMENTS

This paper is an outcome of the EU Interreg IVB project CLIWAT. It has been cofunded by the North Sea Region Programme 2007–2013 under the ERDF of the European Union. This work also was supported by the Danish Agency for Science Technology and Innovation funded project RiskPoint — Assessing the risks posed by point source contamination to groundwater and surface water resources under grant number 09-063216.

A number of students contributed to field work and data collection; particularly, the master student Jesper Pedersen deserves the warmest thanks.

Also, Gianluca Fiandaca is grateful for the support received during the period spent as visiting researcher at Aarhus University (Denmark).

REFERENCES

- Auken, E., and A. V. Christiansen, 2004, Layered and laterally constrained 2D inversion of resistivity data: *Geophysics*, **69**, 752–761, doi: [10.1190/1.1759461](https://doi.org/10.1190/1.1759461).
- Auken, E., A. V. Christiansen, B. H. Jacobsen, N. Foged, and K. I. Sørensen, 2005, Piecewise 1D laterally constrained inversion of resistivity data: *Geophysical Prospecting*, **53**, 497–506, doi: [10.1111/gpr.2005.53.issue-4](https://doi.org/10.1111/gpr.2005.53.issue-4).
- Auken, E., A. Gazoty, G. Fiandaca, J. Pedersen, and A. V. Christiansen, 2011, Mapping of landfills using time-domain spectral induced polarization data — The Eskelund case study: 17th Annual International Conference and Exhibition, EAGE.
- Becker, A., and G. Cheng, 1988, Detection of repetitive electromagnetic signals in electromagnetic methods, in M. N. Nabighian, ed., *Applied Geophysics*: SEG.
- Binley, A., L. D. Slater, M. Fukes, and G. Cassiani, 2005, Relationship between spectral induced polarization and hydraulic properties of saturated and unsaturated sandstone: *Water Resources Research*, **41**, 1–13, doi: [10.1029/2005WR004202](https://doi.org/10.1029/2005WR004202).
- Borner, F. D., J. R. Schopper, and A. Weller, 1996, Evaluation of transport and storage properties in the soil and groundwater zone from induced polarization measurements: *Geophysical Prospecting*, **44**, 583–601, doi: [10.1111/gpr.1996.44.issue-4](https://doi.org/10.1111/gpr.1996.44.issue-4).
- Chen, J., A. Kemna, and S. S. Hubbard, 2008, A comparison between Gauss-Newton and Markov-chain Monte Carlo-based methods for inverting spectral induced-polarization data for Cole-Cole parameters: *Geophysics*, **73**, no. 6, F247–F259, doi: [10.1190/1.2976115](https://doi.org/10.1190/1.2976115).
- Christiansen, A. V., and E. Auken, 2008, Presenting a free, highly flexible inversion code: 78th Annual International Meeting, SEG, Expanded Abstracts, 1228–1232, doi: [10.1190/1.3059140](https://doi.org/10.1190/1.3059140).
- Christiansen, A. V., E. Auken, and A. Viezzoli, 2011, Quantification of modeling errors in airborne TEM caused by inaccurate system description: *Geophysics*, **76**, no. 1, F43–F52, doi: [10.1190/1.3511354](https://doi.org/10.1190/1.3511354).
- Cole, K. S., and R. H. Cole, 1941, Dispersion and absorption in dielectrics: *Journal of Chemical Physics*, **9**, no. 4, 341–351, doi: [10.1063/1.1750906](https://doi.org/10.1063/1.1750906).
- Dahlin, T., C. Bernstone, and M. H. Loke, 2003, A 3-D resistivity investigation of a contaminated site at Lernacken, Sweden: *Geophysics*, **68**, 409, doi: [10.1190/1.1553689](https://doi.org/10.1190/1.1553689).
- Dahlin, T., V. Leroux, and J. Nissen, 2002, Measuring techniques in induced polarisation imaging: *Journal of Applied Geophysics*, **50**, no. 3, 279–298, doi: [10.1016/S0926-9851\(02\)00148-9](https://doi.org/10.1016/S0926-9851(02)00148-9).
- Dahlin, T., and B. Zhou, 2006, Multiple-gradient array measurements for multi-channel 2D resistivity imaging: *Near Surface Geophysics*, **4**, 113–123, doi: [10.3997/1873-0604.2005037](https://doi.org/10.3997/1873-0604.2005037).
- Davidson, D. W., and R. H. Cole, 1951, Dielectric relaxation in glycerol propylene glycol and propanol: *The Journal of Chemical Physics*, **19**, no. 12, 1484–1490, doi: [10.1063/1.1748105](https://doi.org/10.1063/1.1748105).
- Effersø, F., E. Auken, and K. I. Sørensen, 1999, Inversion of band-limited TEM responses: *Geophysical Prospecting*, **47**, 551–564, doi: [10.1046/j.1365-2478.1999.00135.x](https://doi.org/10.1046/j.1365-2478.1999.00135.x).
- Gazoty, A., E. Auken, J. Pedersen, G. Fiandaca, and A. V. Christiansen, 2011, Reliability of time domain induced polarization data: Symposium on the Application of Geophysics to Engineering and Environmental Problems, Charleston.
- Ghorbani, A., C. Camerlynck, N. Florsch, P. Cosenza, and A. Revil, 2007, Bayesian inference of the Cole-Cole parameters from time- and frequency-domain induced polarization: *Geophysical Prospecting*, **55**, 589–605, doi: [10.1111/gpr.2007.55.issue-4](https://doi.org/10.1111/gpr.2007.55.issue-4).
- Hönig, M., and B. Tezkan, 2007, 1D and 2D Cole-Cole-inversion of time-domain induced-polarization data: *Geophysical Prospecting*, **55**, 117–133, doi: [10.1111/gpr.2007.55.issue-1](https://doi.org/10.1111/gpr.2007.55.issue-1).
- Hördt, A., T. Hanstein, M. Hönig, and F. M. Neubauer, 2006, Efficient spectral IP-modelling in the time domain: *Journal of Applied Geophysics*, **59**, no. 2, 152–161, doi: [10.1016/j.jappgeo.2005.09.003](https://doi.org/10.1016/j.jappgeo.2005.09.003).
- Johansen, H. K., and K. I. Sørensen, 1979, Fast Hankel transforms: *Geophysical Prospecting*, **27**, 876–901, doi: [10.1111/gpr.1979.27.issue-4](https://doi.org/10.1111/gpr.1979.27.issue-4).
- Johnson, I. M., 1984, Spectral induced polarization parameters as determined through time-domain measurements: *Geophysics*, **49**, 1993–2003, doi: [10.1190/1.1441610](https://doi.org/10.1190/1.1441610).
- Kemna, A., A. Binley, A. Ramirez, and W. Daily, 2000, Complex resistivity tomography for environmental applications: *Chemical Engineering*

- Journal (Lausanne), **77**, no. 1-2, 11–18, doi: [10.1016/S1385-8947\(99\)00135-7](https://doi.org/10.1016/S1385-8947(99)00135-7).
- Kemna, A., A. Binley, and L. D. Slater, 2004, Crosshole IP imaging for engineering and environmental applications: *Geophysics*, **69**, 97–107, doi: [10.1190/1.1649379](https://doi.org/10.1190/1.1649379).
- Koefoed, O., 1979, *Geosounding principles*: Elsevier.
- Loke, M. H., and R. D. Barker, 1996, Rapid least squares inversion of apparent resistivity pseudosections by a quasi-Newton method: *Geophysical Prospecting*, **44**, 131–152, doi: [10.1111/gpr.1996.44.issue-1](https://doi.org/10.1111/gpr.1996.44.issue-1).
- Loke, M. H., J. Chambers, and R. D. Ogilvy, 2006, Inversion of 2D spectral induced polarization imaging data: *Geophysical Prospecting*, **54**, 287–301, doi: [10.1111/gpr.2006.54.issue-3](https://doi.org/10.1111/gpr.2006.54.issue-3).
- Møller, I., K. I. Sørensen, and N. B. Christensen, 1998, DC-Resistivity multi-electrode profiling in hydrogeological investigations: A comparative study of the pulled array continuous electrical sounding method and a multi-electrode method with fixed electrodes: 11th Symposium on the Application of Geophysics to Engineering and Environmental Problems, EEGS, Extended Abstracts, 869–874.
- Oldenburg, D. W., and Y. Li, 1994, Inversion of induced polarization data: *Geophysics*, **59**, 1327–1341, doi: [10.1190/1.1443692](https://doi.org/10.1190/1.1443692).
- Pelton, W. H., S. H. Ward, P. G. Hallof, W. R. Sill, and P. H. Nelson, 1978, Mineral discrimination and removal of inductive coupling with multifrequency IP: *Geophysics*, **43**, 588–609, doi: [10.1190/1.1440839](https://doi.org/10.1190/1.1440839).
- Revil, A., and N. Florsch, 2010, Determination of permeability from spectral induced polarization in granular media: *Geophysical Journal International*, **181**, 1480–1498, doi: [10.1111/j.1365-246X.2010.04573.x](https://doi.org/10.1111/j.1365-246X.2010.04573.x).
- Seigel, H. O., 1959, Mathematical formulation and type curves for induced polarization: *Geophysics*, **24**, 547–565, doi: [10.1190/1.1438625](https://doi.org/10.1190/1.1438625).
- Shuey, R. T., and M. Johnson, 1973, On the phenomenology of electrical relaxation in rocks: *Geophysics*, **38**, 37–48, doi: [10.1190/1.1440331](https://doi.org/10.1190/1.1440331).
- Slater, L. D., and D. Lesmes, 2002, IP interpretation in environmental investigations: *Geophysics*, **67**, 77–88, doi: [10.1190/1.1451353](https://doi.org/10.1190/1.1451353).
- Slater, L. D., and A. Reeve, 2002, Investigating peatland stratigraphy and hydrogeology using integrated electrical geophysics: *Geophysics*, **67**, 365–378, doi: [10.1190/1.1468597](https://doi.org/10.1190/1.1468597).
- Tarantola, A., and B. Valette, 1982a, Generalized nonlinear inverse problems solved using a least squares criterion: *Reviews of Geophysics and Space Physics*, **20**, no. 2, 219–232, doi: [10.1029/RG020i002p00219](https://doi.org/10.1029/RG020i002p00219).
- Tarantola, A., and B. Valette, 1982b, Inverse problems = quest for information: *Journal of Geophysics*, **50**, no. 3, 159–170, doi: [10.1038/nm1011](https://doi.org/10.1038/nm1011).
- Titov, K., A. Tarasov, Y. Ilyin, N. Seleznev, and A. Boyd, 2010, Relationships between induced polarization relaxation time and hydraulic properties of sandstone: *Geophysical Journal International*, **180**, 1095–1106, doi: [10.1111/gji.2010.180.issue-3](https://doi.org/10.1111/gji.2010.180.issue-3).
- Tombs, J. M. C., 1981, The feasibility of making spectral IP measurements in the time domain: *Geoexploration*, **19**, no. 2, 91–102, doi: [10.1016/0016-7142\(81\)90022-3](https://doi.org/10.1016/0016-7142(81)90022-3).
- Vanhala, H., 1997, Mapping oil-contaminated sand and till with the spectral induced polarization (IP) method: *Geophysical Prospecting*, **45**, 303–326, doi: [10.1046/j.1365-2478.1997.00338.x](https://doi.org/10.1046/j.1365-2478.1997.00338.x).
- Van Voorhis, G. D., P. H. Nelson, and T. L. Drake, 1973, Complex resistivity spectra of porphyry copper mineralization: *Geophysics*, **38**, 49–60, doi: [10.1190/1.1440333](https://doi.org/10.1190/1.1440333).
- Weller, A., W. Frangos, and M. Seichter, 1999, Three-dimensional inversion of induced polarization data from simulated waste: *Journal of Applied Geophysics*, **41**, no. 1, 31–47, doi: [10.1016/S0926-9851\(98\)00036-6](https://doi.org/10.1016/S0926-9851(98)00036-6).
- Weller, A., M. Seichter, and A. Kampke, 1996, Induced-polarization modelling using complex electrical conductivities: *Geophysical Journal International*, **127**, 387–398, doi: [10.1111/gji.1996.127.issue-2](https://doi.org/10.1111/gji.1996.127.issue-2).
- Yoshioka, K., and M. S. Zhdanov, 2005, Three-dimensional nonlinear regularized inversion of the induced polarization data based on the Cole-Cole model: *Physics of the Earth and Planetary Interiors*, **150**, 29–43, doi: [10.1016/j.pepi.2004.08.034](https://doi.org/10.1016/j.pepi.2004.08.034).
- Yuval, , and D. W. Oldenburg, 1997, Computation of Cole-Cole parameters from IP data: *Geophysics*, **62**, 436–448, doi: [10.1190/1.1444154](https://doi.org/10.1190/1.1444154).